Vol. 41 — N° 3 09 17 p. 449–457

GEOSTANDARDS and GEOANALYTICAL RESEARCH

Electron Probe Microanalysis of Bromine in Minerals and Glasses with Correction for Spectral Interference from Aluminium, and Comparison with Microbeam Synchrotron X-Ray Fluorescence Spectrometry

Chao **Zhang** (1)*, Jinru **Lin** (2), Yuanming **Pan** (2), Renfei **Feng** (3), Renat R. **Almeev** (1) and Francois **Holtz** (1)

(1) Institute of Mineralogy, Leibniz Universität Hannover, Hannover, 30167, Germany
(2) Department of Geological Sciences, University of Saskatchewan, Saskatoon, Saskatchewan, S7N 5E2, Canada
(3) Canadian Light Source, University of Saskatchewan, Saskatoon, Saskatchewan, S7N 0X4, Canada
* Corresponding author. e-mail: c.zhang@mineralogie.uni-hannover.de

The strong spectral interference between Br- and Al-induced X-ray lines hampers the utilisation of electron probe microanalysis (EPMA) for measuring Br mass fractions in Al-bearing minerals and glasses. Through measuring Br-free Al-bearing materials, we established an EPMA method to quantify the overlap from Al*Kα* on Br*Lβ*, which can be expressed as a linear function of the Al_2O_3 content. The count rate of the Br*Lβ* peak signal was enhanced by high beam currents and long measurement times. Application of this EPMA method to Al- and Br-bearing materials, such as sodalite and scapolite, and to five experimental glasses yielded Br mass fractions (in the range of 250–4000 μg g^{-1}) that are consistent with those measured by microbeam synchrotron X-ray fluorescence (μ-SXRF) spectrometry. The EPMA method has an estimated detection limit of ~ 100–300 μg g^{-1}. We propose that this method is useful for measuring Br mass fractions (hundreds to thousands of μg g^{-1}) in Al-bearing minerals and glasses, including those produced in Br-doped experiments. In addition, the natural marialitic scapolite (ON70) from Mpwapwa (Tanzania) containing homogeneously distributed high mass fractions of Br (2058 ± 56 μg g^{-1}) and Cl (1.98 ± 0.03% *m/m*) is an ideal reference material for future *in situ* analyses.

Keywords: electron probe microanalysis, synchrotron X-ray fluorescence spectrometry, bromine, aluminium, interference.

Received 24 Nov 16 – Accepted 27 Feb 17

Halogens (F, Cl, Br and I) are common elements and important metal complexing agents in hydrothermal, metamorphic and magmatic systems. Compared with F and Cl, Br is usually several orders of magnitude less abundant in hydrous minerals (e.g., apatite, biotite and amphibole) and in silicate glasses. Consequently, investigations on the behaviour of Br in geological processes are relatively rare, because they require accurate determinations of Br mass fractions in solid phases (minerals and glasses) ranging from 100 μg g^{-1} to < 1 μg g^{-1} (e.g., Pan and Dong 2003, Teiber *et al.* 2014). Little knowledge has been revealed on the partitioning behaviour of Br in magmatic and hydrothermal systems, and there are only a few experiments that studied the partitioning of Br between apatite and fluids/melts (e.g., Dong 2005, Kusebauch *et al.* 2015). Currently, several methods have been applied to measure Br mass fractions in solid phases, including (a) proton-induced X-ray emission (e.g., Vanko *et al.* 2001), (b) microbeam X-ray fluorescence (μ-XRF) spectrometry (e.g., Pan and Dong 2003, Bernal *et al.* 2017), (c) pyrohydrolysis extraction and ion chromatographic quantification (e.g., Köhler *et al.* 2009), (d) instrumental neutron activation analysis (INAA) (e.g., Pan and Dong 2003, Marks *et al.* 2012, Cadoux *et al.* 2017), (e) total reflection X-ray fluorescence spectroscopy (e.g., Marks *et al.* 2012), (f) secondary ion mass spectrometry (e.g., Marks *et al.* 2012, Kusebauch *et al.* 2015, Cadoux *et al.* 2017), (g) laser ablation ICP-MS (e.g., Hammerli *et al.* 2013, 2014, Cadoux *et al.* 2017), (h) noble gas method (e.g., Kendrick 2012) and (i) electron probe microanalysis (EPMA) (e.g., Dong 2005). Among these methods, despite the easiest

doi: 10.1111/ggr.12169
© 2017 The Authors. Geostandards and Geoanalytical Research © 2017 International Association of Geoanalysts

access of EPMA instruments and its highest spatial resolution, determination of Br by EPMA is severely hampered because of the very low intensity of the characteristic X-ray emission and very strong spectral interference between Br- and Al-induced X-ray lines. In this study, we present a new analytical protocol for measuring trace level Br (hundreds to thousands of $\mu g\ g^{-1}$) in Al-bearing minerals and glasses using EPMA. The method was tested by comparing Br mass fractions measured by EPMA and by microbeam synchrotron X-ray fluorescence (μ-SXRF). The EPMA method is shown to be useful for measuring trace level Br in Al-bearing minerals and silicate glasses.

Experimental procedures

Br- and Al-bearing minerals and glasses

The Br- and Al-materials used for EPMA in this study include two minerals and five experimental glasses. One mineral is a sodalite (SOD-1) from South Africa, and its Br mass fraction has been measured by both INAA and μ-XRF at 234 and 221 ± 8 $\mu g\ g^{-1}$, respectively (Pan and Dong 2003). We note that the location of this sample was mixed up with that of another sodalite sample (Bancroft, Ontario, Canada) in Pan and Dong (2003). Another mineral is a marialitic scapolite (ON70) from Mpwapwa, Tanzania (Evans *et al.* 1969, Teertstra and Sherriff 1997), and its Br mass fraction has been measured by μ-SXRF (see below) as 1877 ± 12 $\mu g\ g^{-1}$. The other five experimental glasses have been synthesised at 500 MPa in an internally heated pressure vessel (IHPV, see details in Berndt *et al.* 2002) at the Institute of Mineralogy, Leibniz University of Hannover, Germany. These glasses have been prepared in the course of an experimental project focussing on investigations of the partitioning of F, Cl and Br between silicate melts and amphibole, biotite and apatite at magmatic conditions. The used starting materials consist of two glass powders, and their compositions are as follows: (a) a natural tephriphonolite PF-22 from La Palma (Wengorsch 2013), and (b) a synthetic ferrobasalt SC-1 (Botcharnikov *et al.* 2008). Fluorine was introduced into the system by mixing the two starting glasses with a synthetic F-rich pegmatite glass (4.8% *m/m* F, Bartels *et al.* 2013), and the fraction of F-rich pegmatite in the final glass mixture was 10% or 3%. Chlorine and Br were introduced into the system by adding KCl (or NaCl) and HBr solutions. The mixed glass powder and liquid were sealed in Au capsules, and placed in IHPV for experimental run at 5 kbar and 975 °C for 5 days. The experiments were successfully quenched by dropping down the sample to a cold zone (~ 60 °C), with a quench rate of *ca.* 150 °C s^{-1}. Small fragments of the experimental products were mounted in epoxy, polished and coated with carbon for EPMA. Double-polished wafers (*ca.* 100 μm in thickness) were prepared for μ-SXRF. The experimental products consisted of glass plus minerals (biotite, amphibole, clinopyroxene, apatite and/or ilmenite) (see Figures S1–S5), and their homogenous compositions over the whole capsule indicate crystallisation at near-equilibrium conditions (see glass compositions in Table S1).

Microbeam synchrotron X-ray fluorescence (μ-SXRF) analysis

Microbeam synchrotron X-ray fluorescence (μ-SXRF) measurements were conducted at the *Very Sensitive Elemental and Structural Probe Employing Radiation from a Synchrotron* (VESPERS) beamline at Canadian Light Source (CLS) (Feng *et al.* 2007, 2010). A protocol for Br determination using the μ-SXRF at CLS was developed in this study. A similar measurement method for Br mass fraction using μ-SXRF was recently reported by Cadoux *et al.* (2017). In this study, a 15 keV monochromatic X-ray beam, provided by a double multi-layer monochromator with a band pass of 1.6% and a beam size of 6 μm × 6 μm, was chosen for the measurements. The characteristic X-ray fluorescence spectrum emitted from the sample (Figure 1) was recorded using a four-element Vortex silicon drift detector (Hitachi High-Technologies Science America, Northridge, CA, USA), which was placed ~ 50 mm away from the sample. The detector was positioned 45° to the sample and 90° to the incoming X-ray beam within the polarisation plane (horizontal plane). The flux of the X-ray beam was monitored continuously by ion chambers filled with nitrogen (N_2) gas. In addition, measurements were also made using a polychromatic X-ray beam, covering the energy range of ~ 5–20 keV with a beam size of 3 μm × 3 μm, for comparison. In this case, the experimental set-up was the same as the one used for monochromatic beam measurement, but the Vortex detector was placed ~ 140 mm away from the sample, and the intermediate slit was cut down to 0.1 mm × 0.1 mm.

The samples in the form of doubly polished plates at a thickness of ~ 100 μm, measured using a Mitutoyo thickness gauge, were floated onto a metal-free Lexan film and fixed by Kapton tape, then mounted 45° to the incoming X-ray beam on a motorised XYZ scanning stage. Raster scans were performed over an area of a hundred micrometres (square) using an incident X-ray photon energy of 15 keV for 1 s per pixel, in step sizes of 5–10 μm. At each pixel, in addition to full X-ray fluorescence spectra recorded (Figure 1), the intensities of Cl*K*α, Ca*K*α and Ca*K*β, Ti*K*α and Ti*K*β, Mn*K*α, Fe*K*α and Fe*K*β, Br*K*α and Br*K*β peaks were determined, dead-time corrected and normalised (to the incoming flux) to generate the elemental distribution maps (Figure 2). The average intensity of all pixels from monochromatic measurements

© 2017 The Authors. Geostandards and Geoanalytical Research © 2017 International Association of Geoanalysts

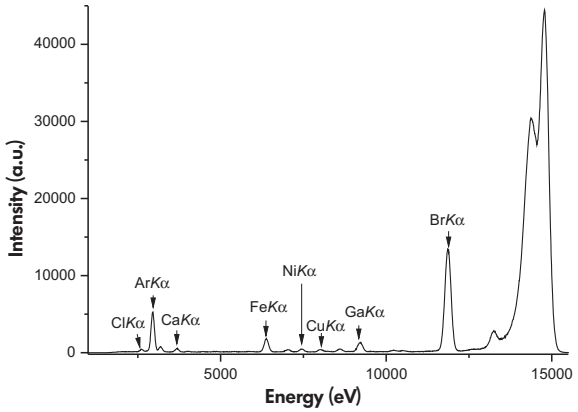

Figure 1. Representative μ-SXRF spectrum of sodalite (SOD-1), measured using a 15 keV monochromatic X-ray beam, illustrating the well resolved Br*K*α peak at ~ 11.9 keV. Other visible peaks are also labelled.

was then used to calculate the elemental mass fractions, using the Br content of SOD-1 from INAA (Pan and Dong 2003) as a measurement standard (see below).

Figure 1 shows that the Br*K*α peaks in the XRF spectra of the sodalite sample (SOD-1), measured using both the polychromatic and monochromatic X-ray beams, are well resolved and have negligible backgrounds. Figure 2 shows that both samples SOD-1 and ON70 are highly homogeneous in the distribution of Br (i.e., standard deviations in the measured intensities < 2%). The use of SOD-1 as a reference material has been confirmed by μ-SXRF measurements of two other minerals (AP-2, chlorapatite, Bob's Lake, Ontario; and SCP-2, marialitic scapolite, Haliburton, Ontario; Pan and Dong 2003) and three Br-doped albite glasses (Figure 3), which were synthesised from melting of Na_2CO_3-Al_2O_3-SiO_2 (molar ratio at 1:1:6) mixtures in platinum crucibles at 1200 °C and atmospheric pressure for 48 h. INAA analyses of the three Br-doped albite glasses (Code 5S at Activation Laboratories Ltd., Ancaster, Ontario, Canada) yielded 4330, 2480 and 466 μg g^{-1} Br; Table 1). The significant variations of the three Br-doped albite glasses obtained from μ-SXRF measurements (~ 10%) can be attributed to the presence of submicrometre-sized cavities (vesicles?) in these samples. The Br mass fractions of scapolite ON70 and the five experimental glasses obtained from monochromatic μ-SXRF measurements, using SOD-1 as a reference material, are compared with the results of EPMA (see below).

Electron probe microanalysis (EPMA)

The EPMA method for measuring trace level Br described in this study was tested using a Cameca SX100 instrument at the Institute of Mineralogy, Leibniz University of Hannover,

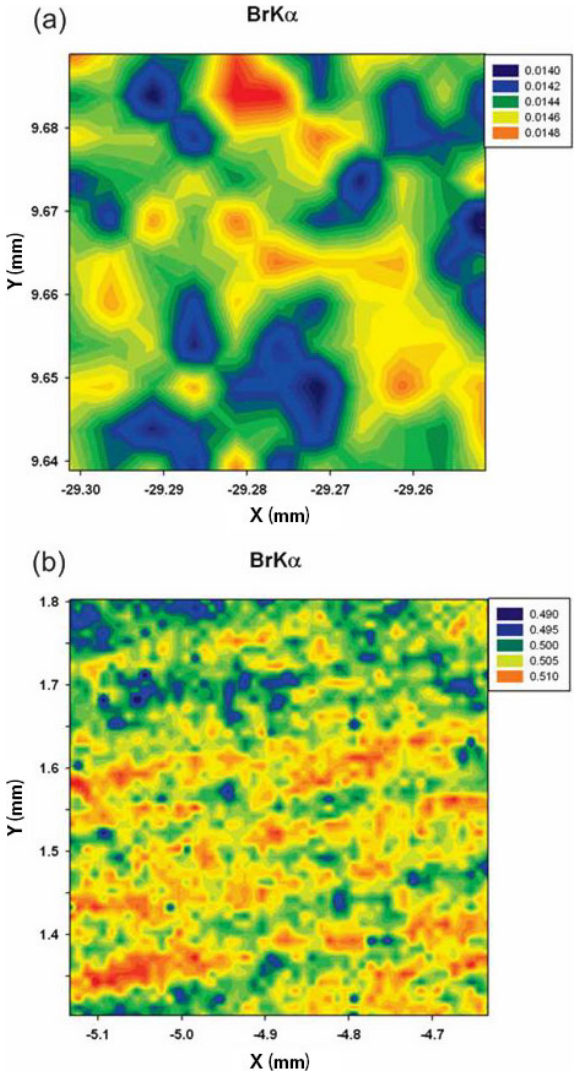

Figure 2. Representative μ-SXRF maps of Br*K*α in (a) sodalite (SOD-1), measured in an area of 50 μm × 50 μm with a monochromatic X-ray beam, note that the obtained Br*K*α intensities of 120 spot analyses varied from 0.0140 to 0.0148 with a standard deviation of 1.38%; and (b) scapolite (ON70), measured in an area of 500 × 500 μm with a polychromatic X-ray beam, the Br intensities for 2600 spot analyses varied from 0.49 to 0.51 with a standard deviation of 0.67%. [Colour figure can be viewed at wileyonlinelibrary.com]

Germany. The EPMA instrument was equipped with five spectrometers and the program *PeakSight*, and the analyses were performed with a 15 keV operating voltage and the 'PAP' matrix correction after Pouchou and Pichoir (1991). High beam currents (100 and 200 nA) and long measurement times (120 s at peak and 60 s at background) were utilised for detecting trace level Br (see below). Synthetic KBr and Al_2O_3 were used as reference materials for quantifying Br and Al signals.

© 2017 The Authors. Geostandards and Geoanalytical Research © 2017 International Association of Geoanalysts

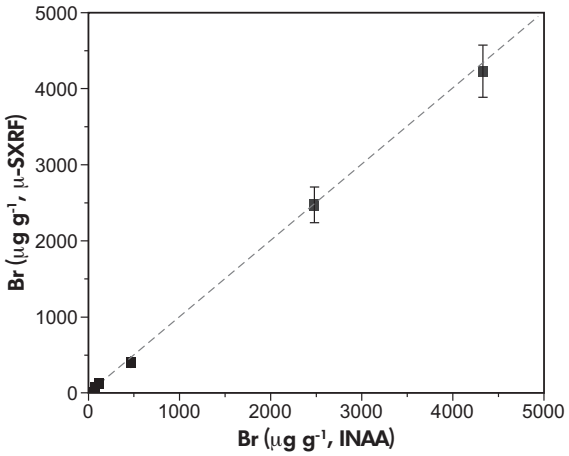

Figure 3. Comparison of Br mass fractions of two mineral samples (AP-2 and SCP-2) and three Br-doped albite glasses from INAA and μ-SXRF analyses (using the SOD-1 as a reference material). The dashed line is the 1:1 line.

Table 1.
Bromine mass fractions of reference materials analysed by INAA and μ-SXRF

Sample	Br (INAA)	Br (μ-SXRF)	
	μg g^{-1}	μg g^{-1}	*s*
Chlorapatite (AP-2)	75[a]	66	1
Scapolite (SCP-2)	115[a]	124	2
Sodalite (SOD-1)	234[a]	234	3
Br-Glass (#1)	4333	4230	342
Br-Glass (#2)	2480	2470	234
Br-Glass (#3)	466	404	42

Br-glasses in this table are Br-doped albite glasses synthesised at atmospheric pressure (see text for details).
[a] INAA analyses from Pan and Dong (2003).

There is a strong spectral interference between the X-ray lines induced from Br and Al (Figure 4), which results in large uncertainties in quantifying the Br signal. This is illustrated by the spectral scan of a synthetic crystal of the end-member $Na_8(Al_6Ge_6)O_{24}Br_2$ (Fleet 1989) (Figure 4a). With the diffraction crystal of thallium acid phthalate (TAP), there are two major Br-induced X-ray lines of Br*L*α (peak position at sinθ = 0.32600) and Br*L*β (peak position at sinθ = 0.31629), which are adjacent to two significant Al-induced X-ray lines of Al*K*α and Al*K*β and their satellite lines (i.e., Als*K*α and Als*K*β). Optimisation of pulse height analysis (PHA) setting (e.g., Zhang *et al.* 2016) cannot be used for diminishing the Al-induced spectral interference, because both Br- and Al-induced X-ray lines are of first order. Importantly, the peaks of Br*L*α and Al*K*α are so close

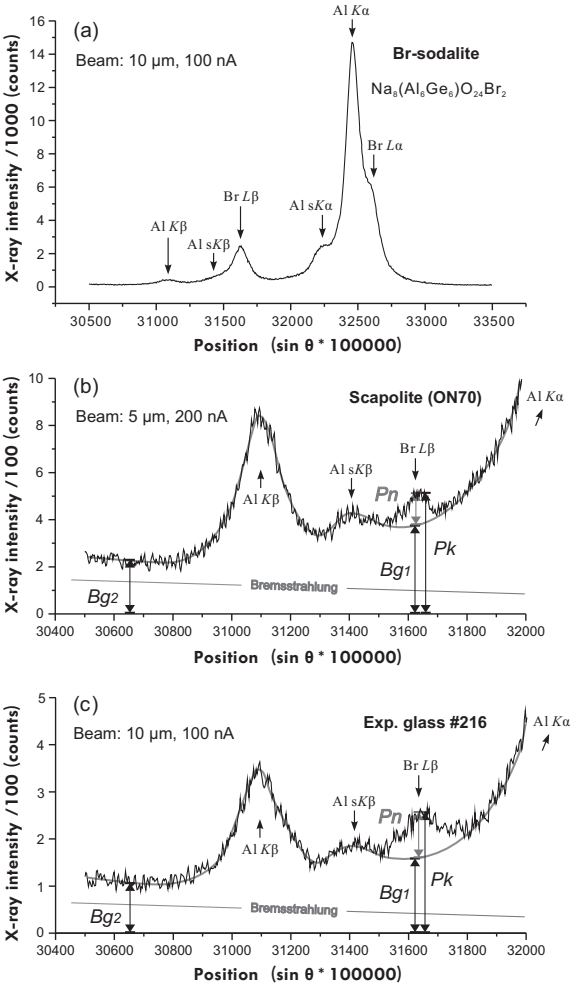

Figure 4. EPMA spectra showing overlapping X-rays from Br and Al. (a) Br-sodalite ($Na_8(Al_6Ge_6)O_{24}Br_2$). (b) Scapolite (ON70) with *ca.* 2000 μg g^{-1}. (c) Experimental glass #216 with *ca.* 4000 μg g^{-1}. The diffraction crystal was thallium acid phthalate (TAP). The beam setting for each material is denoted in the figure. The scan dwell time was 0.1 s, and the accumulation number was 3. The analytical spot was manually moved during spectral scanning to avoid potential damage due to electron bombardment.

that it is hard to extract accurately the overlap from the Al*K*α signal on Br*L*α. Therefore, Br*L*β is the only chance to quantify the Br signal, even though there is still overlap (but much less) from Al*K*α on Br*L*β. Figures 4b and c are spectral scans for scapolite (ON70) and the experimental glass #216, which show that the signal of Br*L*β with trace level Br can only be quantified if the overlap of Al*K*α on Br*L*β can be corrected.

© 2017 The Authors. Geostandards and Geoanalytical Research © 2017 International Association of Geoanalysts

Figures 4b and c show that the apparent peak height *Pk* is the sum of net peak signal of Br (*Pn*) and the background at the peak position (Bg_1):

$$Pk = Pn + Bg_1 \quad (1)$$

As there is an overlap of the Al*K*α peak at the Br*L*β peak position, the value of Bg_1 should be a function of the beam current, 'Bremsstrahlung', and the intensity of the Al*K*α line. Alternatively, the background value (Bg_2) at the peak position of sinθ = Br*L*β–0.01 (that is 0.30629) has little overlap from the Al*K*α peak. Following the procedure of Zhang *et al.* (2016) (that was applied to correct the spectral interference from Fe*L*α on quantifying F*K*α net signal intensity), we propose that Bg_1 and Bg_2 can be expressed as:

$$Bg_1 = Q * (a_1 + b_1 * X_{Al2O3}) \quad (2)$$

$$Bg_2 = Q * (a_2 + b_2 * X_{Al2O3}) \quad (3)$$

where Q is a function of the beam current, constants a_1 and a_2 account for the 'Bremsstrahlung', and constants b_1 and b_2 account for the intensity of the Al*K*α line assuming a linear relationship with the Al_2O_3 content (X_{Al2O3}).

For Br-free references (in this case, $Pk = Bg_1$), one may quantify the overlap from Al*K*α on Br*L*β via measuring Bg_1 and Bg_2:

$$C^{Br}_{Al-overlap} = \frac{(Bg_1 - Bg_2)}{(I * K)} \quad (4)$$

where $C^{Br}_{Al-overlap}$ is the measured apparent Br mass fraction derived from the Br*L*β intensity fully due to overlap from Al*K*α, I is the beam current, and K is a conversion factor for quantifying Br mass fraction from the count rate. Combing the above equations, we obtain

$$C^{Br}_{Al-overlap} = (a_1 - a_2) * \frac{Q}{K * I} + (b_1 - b_2) * \frac{Q}{K * I} * X_{Al2O3} \quad (5)$$

Assuming that

$$m = (a_1 - a_2) * \frac{Q}{K * I} \quad (6)$$

and

$$n = (b_1 - b_2) * \frac{Q}{K * I} \quad (7)$$

we obtain

$$C^{Br}_{Al-overlap} = m + n * X_{Al2O3} \quad (8)$$

The values of m and n can be determined by linear regression of the data obtained on Br-free Al-bearing reference materials, and the relation between $C^{Br}_{Al-overlap}$ and X_{Al2O3} should be applicable for other Br- and Al-bearing materials.

For Br- and Al-bearing materials (in this case, $Pn = Pk - Bg_1$) with Bg_1 involving overlap from Al*K*α, Bg_1 cannot be measured directly but can only be estimated via the relationship between Bg_1 and X_{Al2O3} that has been determined based on Br-free Al-bearing references (Equation 8). Therefore, the real Br mass fraction (C^{Br}_{real}, corresponding to *Pn*) can be extracted from the measurements of apparent Br mass fraction ($C^{Br}_{measure}$, corresponding to *Pk*) through the relation:

$$C^{Br}_{real} = C^{Br}_{measure} - C^{Br}_{Al-overlap} \quad (9)$$

Because of the low-count rate of the Br*L*β line, a high beam current and a long measurement time are required to obtain resolved peak/background ratios for determining trace level Br, and the signal stability in such conditions needs to be tested. We examined the signal stability using a beam size of 5 μm for minerals and a beam size of 10 μm for glasses, which are practical compromises between obtaining sufficient resolution and reducing sample damage. Figures 5a and b show the relationships between the Al*K*α and Br*L*β signals and counting time for scapolite (ON70) (beam: 5 μm, 200 nA) and for the experimental glass #216 (beam: 10 μm, 100 nA), respectively. It is evident that the count rates increase slightly with time. A similar increasing trend of the Al*K*α signal with time for silicate glasses has been previously reported (e.g., Morgan and London 1996, Zhang *et al.* 2016), which results in the variation of the overlap from Al*K*α on Br*L*β (i.e., $C^{Br}_{Al-overlap}$). In order to accurately estimate $C^{Br}_{Al-overlap}$ as a function of Al_2O_3 content, the effective Al_2O_3 content (X^{ef}_{Al2O3}, which is higher than the real X_{Al2O3}) that contributes to the overlap from Al*K*α on Br*L*β can be determined with consideration of the increasing trend of the Al*K*α signal with time. Different materials may display unequal patterns of such increasing trend for the Al count rate. Hence, we measure X^{ef}_{Al2O3} simultaneously with the measurement of $C^{Br}_{measure}$ using the same high current and long measurement time, using two TAP crystals at different spectrometers, which guarantee that the effective overlap from Al*K*α on Br*L*β is accounted for by X^{ef}_{Al2O3}.

Following the above procedures, we determined $C^{Br}_{Al-overlap}$ for a range of Al_2O_3 contents by measuring several Br-free references, including wollastonite (0.0% *m/m* Al_2O_3), augite (8.37% *m/m* Al_2O_3), albite (19.4% *m/m* Al_2O_3) and anorthite (35.4% *m/m* Al_2O_3) (Table 2). Figures 6a and b show plots of $C^{Br}_{Al-overlap}$ versus X^{ef}_{Al2O3} measured with two different beam settings of 5 μm, 200 nA

© 2017 The Authors. Geostandards and Geoanalytical Research © 2017 International Association of Geoanalysts

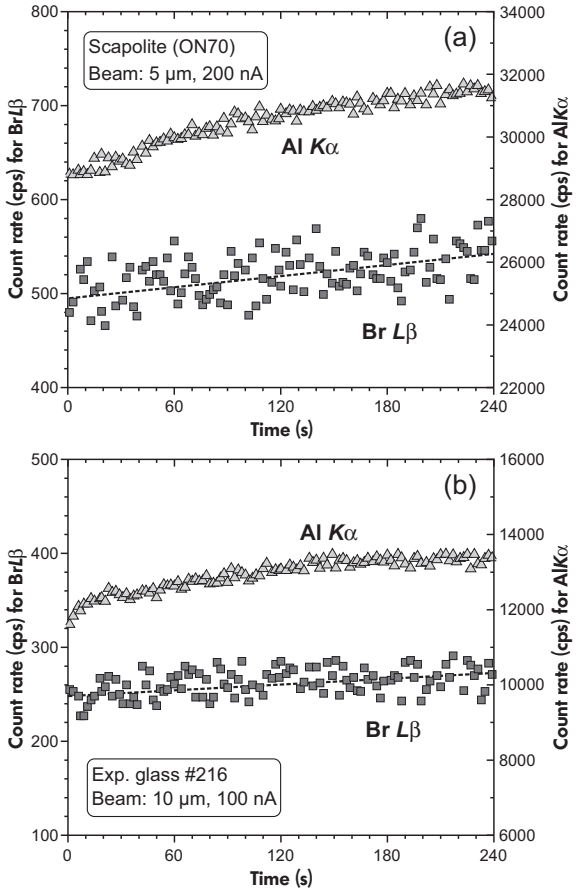

Figure 5. Records of the count rate as a function of time at the wavelength positions of Al*K*α and Br*L*β peaks. (a) Scapolite (ON-70) analysed with a beam of 5 µm and 200 nA. (b) Experimental glass #216 analysed with a beam of 10 µm and 100 nA.

and 10 µm, 100 nA, respectively. For both settings, they display good linear relationships (r^2 values are very close to 1) that are nearly identical to each other, indicating that the used Br-free minerals yield the same $C^{Br}_{Al-overlap}$ using the above beam settings. Although the difference is negligible, we propose that $C^{Br}_{Al-overlap}$ should be determined independently at each measurement session to obtain high accuracy. It is worth noting that both linear relations acquire negative $C^{Br}_{Al-overlap}$ values with $X^{ef}_{Al2O3} = 0$, which reflects the rightward sloping of 'Bremsstrahlung' (Figure 4). In addition, amongst the used four Br-free reference materials, only albite exhibits an apparent discrepancy between measured X^{ef}_{Al2O3} and true Al_2O_3 contents, probably reflecting migration of Na during beam exposure (Reed 2005).

The linear regression results (see Figure 6) are further used to calculate $C^{Br}_{Al-overlap}$ for unknown Br-bearing materials over the range of Al_2O_3 content (at least capable within 0–40% *m/m*). Applying the protocol for the determination of $C^{Br}_{Al-overlap}$ (as a function of Al_2O_3 content, see Equation 8) and C^{Br}_{real} (see Equation 9), we have measured selected Al-bearing materials with trace level Br mass fractions. Sodalite (SOD-1) and scapolite (ON70) have been measured with a beam of 5 µm and 200 nA; five experimental glasses (#213, #215, #216, #217, #218) have been measured with a beam of 10 µm and 100 nA.

Results and discussion

Figure 7 shows that the Br mass fractions of the sodalite and scapolite and the five experimental glasses obtained in this study by the EPMA are in good agreement with those measured using the µ-SXRF method (data in Table 3), thus confirming the high potential of the presented EPMA measurement method. As shown in Table 3, the analytical standard deviation was around 100 µg g^{-1} for Br mass fractions within 1000–4000 µg g^{-1}, or within 20–100 µg g^{-1} for lower Br mass fractions within 100–1000 µg g^{-1}. Because $C^{Br}_{Al-overlap}$ refers to the background for determining true Br mass fractions, the scatter in the measurements of $C^{Br}_{Al-overlap}$ strongly affects the detection limits of the Br determinations. According to the recommendation of Analytical Methods Committee (1987), detection limit corresponds to a peak count that is higher than the mean background count by three times of standard deviation of background count. In this case, the detection limit of Br determinations by EPMA should be calculated as three times of the standard deviation of measured $C^{Br}_{Al-overlap}$

Table 2.
Electron probe microanalyses of Br-free reference minerals

Sample	X_{Al2O3}	X^{ef}_{Al2O3}	$C^{Br}_{Al-overlap}$		X^{ef}_{Al2O3}	$C^{Br}_{Al-overlap}$	
		Beam = 5 µm, 200 nA			Beam = 10 µm, 100 nA		
	% *m/m*	% *m/m*	µg g^{-1}	*s*	% *m/m*	µg g^{-1}	*s*
Wollastonite	0.0	0.0	-365	60	0.0	-363	39
Augite	8.37	8.39	1140	52	8.38	1202	79
Albite	19.4	20.5	3271	60	19.6	3187	71
Anorthite	35.4	35.5	6061	98	35.4	6290	95

© 2017 The Authors. Geostandards and Geoanalytical Research © 2017 International Association of Geoanalysts

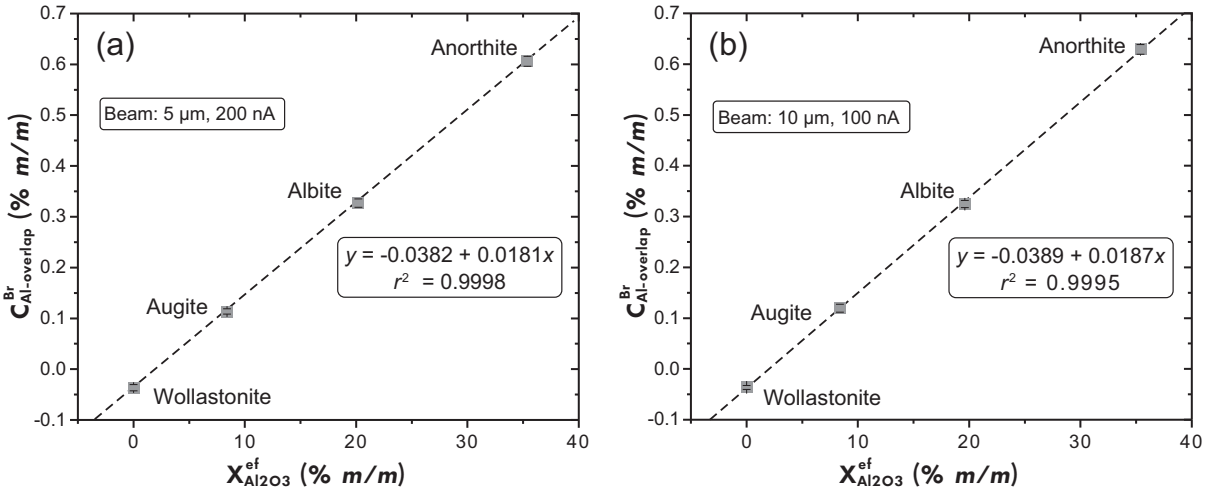

Figure 6. The relationship between the apparent Br mass fraction ($C^{Br}_{Al-overlap}$) and effective Al_2O_3 content (X^{ef}_{Al2O3}). (a) Results with a beam of 5 µm and 200 nA. (b) Results with a beam of 10 µm and 100 nA. The linear regression line and equation are given in the figure. The error bars represent one standard deviation.

(Table 2), i.e., in the range of 120–300 µg g^{-1}. We propose that, with the established EPMA method, Br mass fractions above 1000 µg g^{-1} in unknown materials can be measured readily with high accuracy (see Table 3 and Figure 7), while measuring Br mass fractions below 200 µg g^{-1} (calculated average detection limit) are challenging with notable uncertainty.

Of particular interest is the anomalously high Br mass fraction in scapolite ON70, obtained by both the EPMA and µ-SXRF techniques. The Br and Cl mass fractions of 2058 ± 56 µg g^{-1} and 1.98 ± 0.03% *m/m* from EPMA yield a molar Cl/Br ratio of 223, which is one of the lowest values documented for scapolite in the literature (Pan and Dong 2003, Hammerli *et al.* 2014). Unfortunately, the precise location and mineral assemblage/paragenesis of ON70 scapolite are unknown (Evans *et al.* 1969), precluding an elucidation of the possible origin for the anomalous Cl/Br ratio. On the other hand, both EPMA and µ-SXRF confirm a homogeneous distribution of Br in this sample (Figure 2b), making it a potential reference material for future *in situ* determinations of Br and Cl for EPMA and other analytical techniques (e.g., µ-SXRF, LA-ICP-MS and SIMS).

Conclusions

The spectral interference from Al-induced X-ray lines on the Br*L*β peak in electron probe microanalyses has been quantified as a function of Al_2O_3 contents through measuring Br-free Al-bearing references, and its application to Br- and Al-bearing unknowns enables measuring trace level Br. High beam currents and long measurement times are necessary to overcome the low-count rate of the Br X-ray line. Bromine mass fractions of two minerals and five experimental glasses, within a range of 250–4000 µg g^{-1}, have been measured by both EPMA and µ-SXRF methods. A good

Table 3.
EPMA and µ-SXRF analyses of Al- and Br-bearing minerals and glasses

Sample	Al_2O_3	Br (µ-SXRF)		Br (EPMA)	
	% *m/m*	Mean	*s*	Mean	*s*
Sodalite (SOD-1)	33.1	234[a]	3	248	29
Scapolite (ON70)	23.9	1877	12	2058	56
Exp. glass #213	18.3	1035	10	1131	95
Exp. glass #215	18.1	2346	23	2309	115
Exp. glass #216	18.5	4012	40	3974	82
Exp. glass #217	14.8	1957	20	2074	48
Exp. glass #218	15.0	3285	33	3372	88

Br mass fraction in µg g^{-1}. Experimental glasses were synthesised at 5 kbar, at the University of Hannover, Germany (see text for details). For EPMA data, sodalite and scapolite were measured with beam of 5 µm and 200 nA, whereas the five experimental glasses were measured with beam of 10 µm and 100 nA. For data analysed with µ-SXRF, mean and standard deviation were derived from 2600 spot analyses (scapolite ON70) or 120 spot analyses (sodalite SOD-1 and experimental glasses) (see also Figure 2). For data analysed with EPMA, mean and standard deviation were derived from ten spot analyses.

[a] The sodalite (SOD-1) Br mass fraction from INAA analysis (Pan and Dong 2003) was used as a measurement standard for µ-SXRF at Canadian Light Source, University of Saskatchewan, Canada.

© 2017 The Authors. Geostandards and Geoanalytical Research © 2017 International Association of Geoanalysts

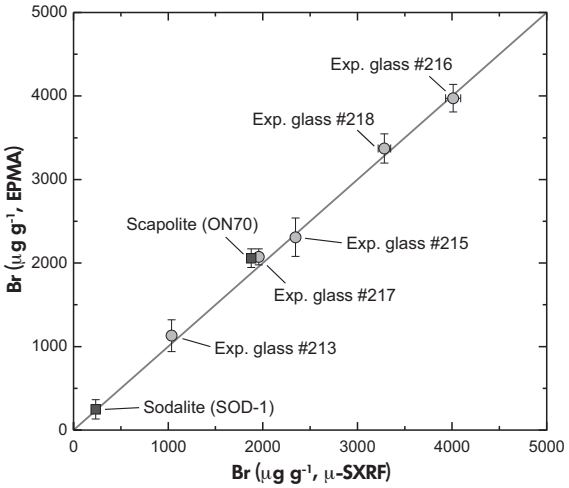

Figure 7. Comparison of Br mass fractions measured by EPMA and μ-SXRF. The Br mass fraction of sodalite (SOD-1) is after Pan and Dong (2003). The other data were obtained in this study (see text for details). The grey line is the 1:1 line. The error bars represent two standard deviations.

agreement between the two methods demonstrates the capability and potential of the presented EPMA method for measuring trace level Br in minerals and glasses. Although very low Br mass fractions (< 100 μg g^{-1}) may not be measured accurately by the EPMA method described in this paper, we believe this method should be useful for measuring trace level Br mass fractions (hundreds to thousands of μg g^{-1}) in some minerals and glasses formed in Br-doped experiments. The natural marialitic scapolite (ON70) from Mpwapwa (Tanzania) containing homogeneously distributed high mass fractions of Br (2058 ± 56 μg g^{-1}) and Cl (1.98 ± 0.03% *m/m*) is an optimal reference material for future *in situ* analyses.

Acknowledgements

We thank two anonymous journal reviewers for helpful comments and Kathryn Linge for editorial handling. We also thank Prof. Jürgen Koepke (LUH) for inspiring discussions. This study was supported by a 'Wege in die Forschung' project (granted by Leibniz Universität Hannover to Chao Zhang) and DFG (German Research Foundation) project BE 1720/40.

References

Analytical Methods Committee (1987)
Recommendations for the definition, estimation and use of the detection limit. **Analyst**, 112, 199–204.

Bartels A., Behrens H., Holtz F., Schmidt B.C., Fechtelkord M., Knipping J., Crede L., Baasner A. and Pukallus N. (2013)
The effect of fluorine, boron and phosphorus on the viscosity of pegmatite forming melts. **Chemical Geology**, 346, 184–198.

Bernal N.F., Gleeson S.A., Smith M.P., Barnes J.D. and Pan Y. (2017)
Evidence of multiple halogen sources in scapolites from iron oxide-copper-gold (IOCG) deposits and regional NaCl metasomatic alteration, Norrbotten County, Sweden. **Chemical Geology**, 451, 90–103.

Berndt J., Liebske C., Holtz F., Freise M., Nowak M., Ziegenbein D., Hurkuck W. and Koepke J. (2002)
A combined rapid-quench and H_2-membrane setup for internally heated pressure vessels: Description and application for water solubility in basaltic melts. **American Mineralogist**, 87, 1717–1726.

Botcharnikov R.E., Almeev R.R., Koepke J. and Holtz F. (2008)
Phase relations and liquid lines of descent in hydrous ferrobasalt – Implications for the Skaergaard intrusion and Columbia River flood basalts. **Journal of Petrology**, 49, 1687–1727.

Cadoux A., Iacono-Marziano G., Paonita A., Deloule E., Aiuppa A., Eby G.N., Costa M., Brusca L., Berlo K., Geraki K., Mather T.A., Pyle D.M. and Di Carlo I. (2017)
A new set of standards for *in-situ* measurement of bromine abundances in natural silicate glasses: Application to SR-XRF, LA-ICP-MS and SIMS techniques. **Chemical Geology**, 452, 60–70.

Dong P. (2005)
Halogen-element (F, Cl, and Br) behaviour in apatites, scapolite, and sodalite: An experimental investigation with field applications. **Ph.D. thesis, University of Saskatchewan** (Saskatoon), 234pp.

Evans B.W., Shaw D.M. and Haughton D.R. (1969)
Scapolite stoichiometry. **Contributions to Mineralogy and Petrology**, 24, 293–305.

Feng R., Gerson A., Ice G., Reininger R., Yates B. and McIntyre S. (2007)
VESPERS: A beamline for combined XRF and XRD measurements. **AIP Conference Proceedings**, 879, 872–874.

Feng R., Dolton W., Igarashi R., Wright G., Bradford M. and McIntyre S. (2010)
Commissioning of the VESPERS beamline at the Canadian Light Source. **AIP Conference Proceedings**, 1234, 315–318.

Fleet M. (1989)
Structures of sodium alumino-germinate sodalites $[Na_8(Al_6Ge_6O_{24})A_2$, A = Cl, Br, I]. **Acta Crystallographica, C45**, 843–847.

© 2017 The Authors. Geostandards and Geoanalytical Research © 2017 International Association of Geoanalysts

references

Hammerli J., Rusk B., Spandler C., Emsbo P. and Oliver N.H.S. (2013)
In situ quantification of Br and Cl in minerals and fluid inclusions by LA-ICP-MS: A powerful tool to identify fluid sources. Chemical Geology, 337–338, 75–87.

Hammerli J., Spandler C., Oliver N.H.S. and Rusk B. (2014)
Cl/Br of scapolite as a fluid tracer in the Earth's crust: Insights into fluid sources in the Mary Kathleen Fold Belt, Mt. Isa Inlier, Australia. Journal of Metamorphic Geology, 32, 93–112.

Kendrick M.A. (2012)
High precision Cl, Br and I determinations in mineral standards using the noble gas method. Chemical Geology, 292–293, 116–126.

Köhler J., Schönenberger J., Upton B. and Markl G. (2009)
Halogen and trace-element chemistry in the Gardar Province, South Greenland: Subduction-related mantle metasomatism and fluid exsolution from alkalic melts. Lithos, 113, 731–747.

Kusebauch C., John T., Whitehouse M.J., Klemme S. and Putnis A. (2015)
Distribution of halogens between fluid and apatite during fluid-mediated replacement processes. Geochimica et Cosmochimica Acta, 170, 225–246.

Marks M.A.W., Wenzel T., Whitehouse M.J., Loose M., Zack T., Barth M., Worgard L., Krasz V., Eby G.N., Stosnach H. and Markl G. (2012)
The volatile inventory (F, Cl, Br, S, C) of magmatic apatite: An integrated analytical approach. Chemical Geology, 291, 241–255.

Morgan G.B. VI and London D. (1996)
Optimizing the electron microprobe analysis of hydrous alkali aluminosilicate glasses. American Mineralogist, 81, 1176–1185.

Pan Y. and Dong P. (2003)
Bromine in scapolite-group minerals and sodalite: XRF microprobe analysis, exchange experiments, and application to skarn deposits. The Canadian Mineralogist, 41, 529–540.

Pouchou J.L. and Pichoir F. (1991)
Quantitative analysis of homogeneous or stratified microvolumes applying the model "PAP". In: Heinrich K.F.J. and Newbury D.E. (eds), Electron probe quantitation. Plenum Press (New York, USA), 31–75.

Reed S.J.B. (2005)
Electron microprobe analysis and scanning electron microscopy in geology (2nd Edition). Cambridge University Press (Cambridge, UK), 232pp.

Teertstra D.K. and Sherriff B.L. (1997)
Substitutional mechanisms, compositional trends and the end-member formulae of scapolite. Chemical Geology, 136, 233–260.

Teiber H., Marks M.A.W., Wenzel T., Siebel W., Altherr R. and Markl G. (2014)
The distribution of halogens (F, Cl, Br) in granitoid rocks. Chemical Geology, 374–375, 92–109.

Vanko D.A., Bonnin-Mosbah M., Philippot P., Roedder E. and Sutton S.R. (2001)
Fluid inclusions in quartz from oceanic hydrothermal specimens and the Bingham, Utah porphyry-Cu deposit: A study with PIXE and SXRF. Chemical Geology, 173, 227–238.

Wengorsch T. (2013)
Experimental constraints on the storage conditions of a tephriphonolite from the Cumbre Vieja volcano (La Palma, Canary Islands) at 200 and 400 MPa. M.Sc. thesis, Leibniz Universität Hannover (Hannover, Germany), 97pp.

Zhang C., Koepke J., Wang L.-X., Wolff P.E., Wilke S., Stechern A., Almeev R. and Holtz F. (2016)
A practical method for accurate measurement of trace level fluorine in Mg- and Fe-bearing minerals and glasses using electron probe microanalysis. Geostandards and Geoanalytical Research, 40, 351–363.

Supporting information

The following supporting information may be found in the online version of this article:

Figures S1–S5. Backscattered electron images of experimental target materials.

Table S1. EPMA data of experimental glasses.

This material is available as part of the online article from: http://onlinelibrary.wiley.com/doi/10.1111/ggr12169/ abstract (This link will take you to the article abstract).

© 2017 The Authors. Geostandards and Geoanalytical Research © 2017 International Association of Geoanalysts